



Seismic de-multiple strategy in the submarine slope of Taiwan accretionary wedge

Feisal Dirgantara, Andrew Tien-Shun Lin & Char-Shine Liu

To cite this article: Feisal Dirgantara, Andrew Tien-Shun Lin & Char-Shine Liu (2022): Seismic de-multiple strategy in the submarine slope of Taiwan accretionary wedge, *Exploration Geophysics*, DOI: [10.1080/08123985.2022.2086040](https://doi.org/10.1080/08123985.2022.2086040)

To link to this article: <https://doi.org/10.1080/08123985.2022.2086040>



Published online: 10 Jun 2022.



Submit your article to this journal



View related articles



View Crossmark data



Seismic de-multiple strategy in the submarine slope of Taiwan accretionary wedge

Feisal Dirgantara^{a,b,c}, Andrew Tien-Shun Lin^{b,c} and Char-Shine Liu^d

^aInstitute of Earth Sciences, Academia Sinica, Taipei, Taiwan; ^bTaiwan International Graduate Program – Earth System Science Program, Academia Sinica, Taipei, Taiwan; ^cDepartment of Earth Sciences, National Central University, Taoyuan, Taiwan; ^dOcean Center, National Taiwan University, Taipei, Taiwan

ABSTRACT

Reducing multiple contaminations in reflection seismic data remains one of the primary challenges in marine seismic data processing. Besides geological settings, its effectiveness is also dependent on the multiple removal methods. In this study, we undertook two legacy 2D multi-channel seismic data crossing the accretionary wedge off SW Taiwan to test the efficiency of various multiple-attenuation scenarios. The tectonic domain has resulted from the incipient arc-continent collision between the northern rifted margin of the South China Sea and the Luzon volcanic arc. The wedge extends from shallow water to deep water bathymetries, hence promoting both short-period and long-period multiples within the seismic records. A cascade of de-multiple methods was tested to attenuate multiple energy under various seafloor bathymetry and tectonic areas. The first step relies on the periodicity nature of multiples. Spatial dependent predictive deconvolution in the x - t domain was performed to attenuate reverberations and improve temporal resolution in the time domain. Wave-equation multiple attenuation (WEMA) was applied to suppress the water layer multiples based on a combination of numerical wave extrapolation in the shot domain through water layer and water bottom reflectivity. Surface-related multiple elimination (SRME) aimed to attenuate the residual water bottom multiple and peg-leg multiple by assuming surface-related multiples can be kinematically predicted via convolution of pre-stack seismic traces at possible surface multiple reflection locations. The second step exploits the spatial move-out difference behavior between primaries and multiples. Parabolic Radon transforms far-offset multiples by subtracting noise energy in the τ - p domain, whereas the frequency-wave number (F-K) filter aimed to eliminate any residual multiples energy in the F-K domain. Predictive deconvolution improved seismic resolution and suppressed sea-bottom reverberation energy in the continental and lower wedge slopes, but not in the upper wedge slope. WEMA, Radon filter, and F-K filter reduced multiples energy both at the continental slope and wedge slope; whereas SRME made minimal impact on both areas. Since the reflection seismic datasets stretch diverse tectonic environments and water depth, there was no single multiple attenuation method capable to suppress multiples in all tectonic environments and bathymetry.

ARTICLE HISTORY

Received 21 July 2021

Accepted 31 May 2022

KEYWORDS

Multi-channel seismic; seismic exploration; seismic processing; multiple attenuation; accretionary wedge; Taiwan

Introduction

In the past decades, multi-channel seismic (MCS) has been relied upon to image medium to large scale structural and stratigraphic features in submarine accretionary wedges (Shipley et al. 1992; Boston et al. 2016). Seismic imaging aims to focus energy back to the reflection points at the interface of inhomogeneities by assuming that all scattered energy has been reflected in the subsurface only once. However, as each interface behaves as a reflector irrespective of the direction of propagation, a propagating wave undergoes several reflections at every interface, hence the promotion of artifacts and noises. In a submarine environment, the presence of artifacts and noises are often associated with acquisition design and water depths (Yilmaz 2008).

Although the standard processing procedures are capable of eliminating artifacts, multiple noises remain one of the greatest problems in marine seismic processing.

Multiple is best described as a secondary, scattering of energy when seismic waves pass through a medium prior to the recording at seismic receivers. Based on the periodicity, multiples are divided as short-period multiples and long-period multiples. The latter multiples are those multiples for which multiple events can be decomposed into primary ray paths, which all have two-way travel times that can be observed as different arrivals in the seismic data. On the other hand, short-period multiples cannot be observed as separate events from the primaries that generate them, hence non-deterministic behavior. Based on the interface where

energy bounces take place, multiples can be categorized as surface-related multiples and internal multiples. The first type infers the energy bounces at least one time at the sea surface, while the second type suggests the energy reverberates with two or more sub-bottom layers. Verschuur (2013) views multiples according to their characteristics, such as (1) periodic repetition of reflection events; (2) conflicting dips with primaries; (3) focusing and defocusing effects due to structural effects in multiple-generating layers; (4) magnification of amplitude effects for higher-order multiples; and (5) interferences effects of multiples and primaries or between different multiples. With similar stacking velocities and travel time with the primary reflections, multiples can plague weak primary reflections from deep targets located below a succession of high- and low-velocity layers (Verschuur and Berkhouw 2015). Based on the algorithm, multiple removal methods can be classified into two groups (Verschuur 2013): (1) methods based on a difference in the spatial behaviour of primaries and multiples; (2) methods based on periodicity and predictability. Data domain transformation is commonly performed to better discriminate noises from desired signals accurately and to mitigate the lack of multiple energy removal by simple stacking (Hampson 1986). Regardless of the preferred attenuation methods, combined tests of several de-multiple techniques are prerequisite to effectively attenuate multiples in different submarine geological settings (Berndt and Moore 1999).

The study area spans from the incipient arc-continent collision between the northern rifted margin of the South China Sea (SCS) and the Luzon volcanic arcs off southwestern Taiwan to the continental slope of the Chinese passive margin (Figure 1). From a geodynamics perspective, Reed et al. (1992) subdivided the incipient collisional wedge into a lower slope domain and an upper slope domain. The upper wedge slope domain is characterized by a series of mud diapirs, weak seismic reflections, and localized active deformation, while the lower wedge slope domain is dominated by thrust-and-fold belts. A deformation front bounds the eastern limit of the SCS continental slope and the lower slope domain. Tectonic features in the SCS continental slope are characterized by normal faults (Liu, Huang, and Teng 1997), whereas fold-and-thrust structures of the convergent zone dominate the orogenic wedge. Both the continental and wedge slope domains are dominated by offscraped continental margin strata and orogenic sediments derived from the Taiwan mountain belts, respectively. As one of only a handful active and young orogen, understanding the subsurface image of Taiwan orogen requires a high-resolution crustal-scale geophysical constraint. Past studies had displayed how extensive efforts of multiple attenuation methods have been tested within the vicinity of the study area. Berndt and Moore (1999) showcased

the usage of F-K (frequency-wave number) filter, Radon filter, wave equation multiple rejection, time variant frequency filter, and deconvolution in southern offshore Taiwan, including the nascent accretionary prism and the Luzon arc area. Lester and McIntosh (2012) demonstrated the effectiveness of 2D surface-related multiple elimination (SRME) and Radon filter in attenuating multiples energy in the eastern Eurasian continental margin, the Manila subduction system, and the Ryukyu trench accretionary prism. Yeh et al (2012) tested the F-K filter, Radon transform, and SRME based on the source structures of multiple occurrences in the north-eastern SCS. Regardless of the method, each lies on assumptions and its effectiveness highly depends on its compatibility with the preconditions (Yilmaz 2008). Acquisition parameters, geometry of the survey, physical properties of the medium, and geological features, all play a pivotal role in the success or failure of these methods.

Upon the aforementioned geological traits of Taiwan wedge slope, an effective, amplitude-preserved processing is paramount to revamp the seismic resolution. The dramatic bathymetry changes from accretionary wedge slope domain to continental slope domain allow the presence of short-period and long-period multiples in the seismic data together with their own imaging challenges. Along the accretionary wedge slope, short-period multiples can be generated and require predictive deconvolution to attenuate energy. Radon filter and F-K filter, which require velocity discrimination, may fail as the multiples are often coincident with primary reflections from shallow lower slope stratification due to the similarity in move-out (Lester and McIntosh 2012). Shallow reflections are often limited with low number of fold coverage, limiting the effectiveness of velocity-based de-multiple methods. Conversely, deep water multiples in the continental slope with a large periodicity do not suit the purpose of predictive deconvolution without damaging the primary reflections. The velocity-based methods can be more effective in such scenarios as different move-outs between multiples and deeper reflections are typically present (Yilmaz 2008). Classified as wave equation-based multiple attenuation, both wave-equation multiple attenuation (WEMA) and surface-related multiple elimination (SRME) perform multiple modeling and adaptive subtraction. Theoretically, both methods should be able to handle multiple attenuations independently, regardless of bathymetry and morphology conditions. Furthermore, several advanced processing techniques, e.g. amplitude-versus-offset (AVO) analysis, velocity model building, and pre-stack/post-stack migration, require the relative amplitudes of seismic data to be preserved without multiples. A prudent multiple attenuation effort is, therefore, necessary to improve the temporal and spatial resolution of a subsurface image. This study attempted to revisit the MCS legacy dataset and test the

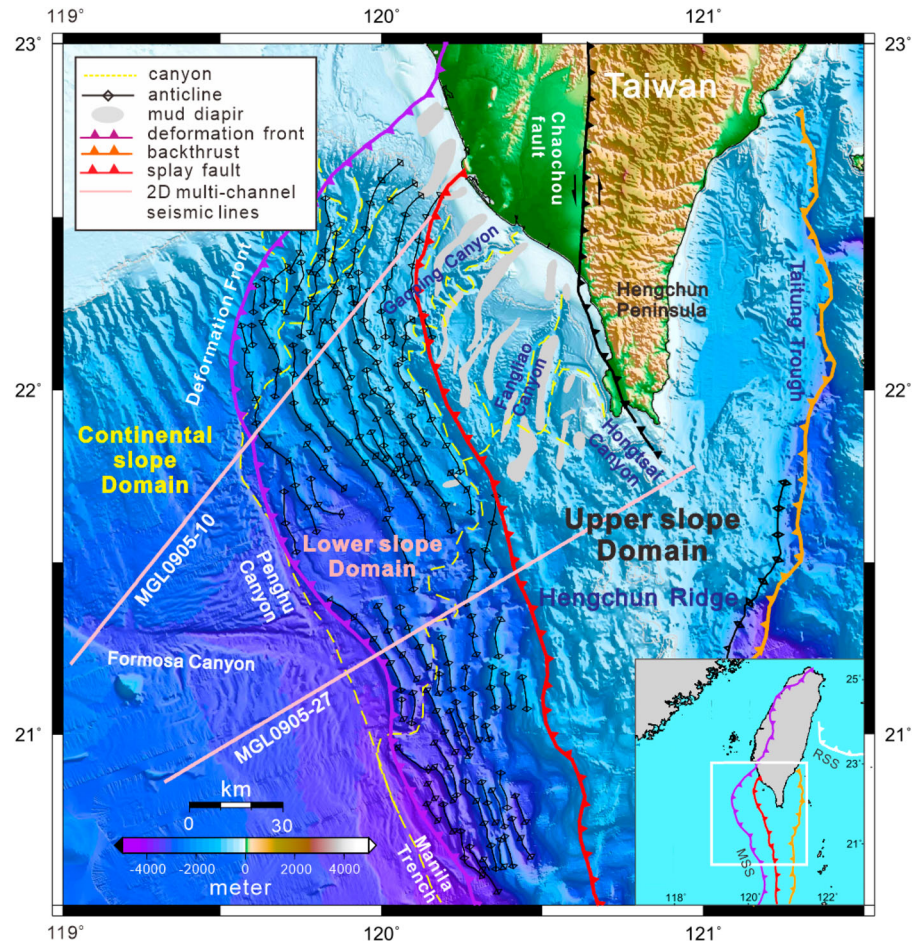


Figure 1. (Bottom, right) Simplified map of Taiwan and the surrounding area showing major tectonic elements. The white square shows the location of the bathymetric map (larger map) of southern Taiwan. Two seismic lines, MGL 0905-10 and MGL 0905-27, are used in this study. MSS: Manila Subduction System. RSS: Ryukyu Subduction System. Offshore structures follow Lin et al. (2008, 2009a) and Dirgantara et al. (2020a).

multiple attenuation strategy in the submarine slope area off southwestern Taiwan. Two 2D MCS profiles were re-processed and presented to demonstrate some of the de-multiple challenges and limitations imposed in the submarine Taiwan accretionary wedge imaging.

Regional geology

The Taiwan island is an active curved collision belt and thrust wedge (Suppe 1981), which developed as a result of the late Cenozoic oblique convergence between the Philippine Sea Plate and the Eurasian Plate, since the late Miocene (Lin, Watts, and Hesselbo 2003) (Figure 1). A convergence rate of 70–86 km/m.y in a northwest fashion has been established from global plate models and GPS data (Seno, Stein, and Gripp 1993; Yu, Chen, and Kuo 1999; Hall 2002). Due to the obliqueness of collision, many viewed the different spatial locations in the orogen to represent the different temporal stages of collision (Suppe 1984; Lee et al. 2006). The areas of offshore southwestern Taiwan are in an initial stage of arc-continent collision, composed by the overriding accretionary wedge and the under-thrusting Eurasian lithosphere (Lin et al. 2009a).

From the northwest-ward off the northern tip of the Manila Trench to the edge of the continental slope, marks a deformation front that separates the horst-and-graben structures of the rifted continental margin from the fold-and-thrust structures of the convergent zone. Underlain by the Tertiary Tainan Basin, the southeastern Chinese passive margin is characterized by well-developed shelf-slope-rise settings, with slope bathymetry that lies between 200 and 3000 m isobaths (Teng 1990), slope gradient that ranges from 0.2° to 5.6° (Gong et al. 2015; Liao et al. 2016), and an extensive deposition of sediment waves (Ludmann et al. 2001). Active deepwater channels, submarine canyons, and slope gullies play instrumental roles in the transportation and distribution of downslope movements. Formosa Canyon and Penghu Canyon developed from turbidity-current erosion and mass wasting processes in the continental slope and extended downslope, before merging with the Manila Trench.

Imbricated thrust ramps over a gently east-dipping decollement marks the western edge of the two-sided submarine orogeny (Liu, Huang, and Teng 1997). Two structural domains have been recognized on the trench side of the accretionary wedge: an intensely deformed

upper slope domain and a lower slope domain which comprise NNW-trending, mostly the west-vergent ramp anticlines and thrusts (Reed et al. 1992). Gradual changes in the structures trending from NNW-SSE in the lower slope domain to NNE-SSW take place as the fold-thrust belt emerges close to the shallower bathymetry offshore southwestern Taiwan. Reflection seismic imaging reveals a complex system of faults, folds, mud diapirs, sedimentary basins, sediment waves, the presence of bottom simulating reflectors (BSRs), and submarine channels in the area (Liu, Huang, and Teng 1997; Deng et al. 2006; Lin et al. 2008, 2009a, 2009b; Liao et al. 2014; Dirgantara et al. 2020a, 2020b). These reflection profiles were acquired in both strike and dip orientations across the submarine Taiwan accretionary wedge slope and Eurasia continental margin. Liu et al. (2006) viewed contrasting processes modulating the structural patterns in the lower slope domain (by structural shortening) versus the upper slope domain (by structural complexity).

A series of anticlinal ridges generated as fault-bend folds over thrust ramps characterizes the lower slope domain (Liu et al. 2006). Abrupt changes in the wedge structure occur at the slope boundary. An increment of the surface gradient at the boundary reflects the out-of-sequence-thrusting within the wedge and structurally separates both domains (Reed et al. 1992). Highly chaotic and discontinuous reflection of the upper slope implies an intense deformation (Liu et al. 2006). Slope basins are bounded at the rear sides of both thrust ridges of the lower slope and anticlinal ridges of the upper slope, where syn-tectonic sedimentation is presented by progressively tilted reflectors at the basin edges (Lundberg et al. 1992; Yu and Huang 2006; Hsu et al. 2013; Dirgantara et al. 2020a). In the nearshore area of the Taiwan wedge, a series of mud-cored anticlines have developed underlying thick sedimentary layers (Sun and Liu 1993; Liu, Huang, and Teng 1997; Dirgantara et al. 2020a) in the NNE-SSW trend, parallel to the structural trend of faults, folds, and onshore mud volcanoes.

Multi-channel seismic data acquisition and re-processing flow

Two-dimensional long offset MCS data were collected during the summer of 2009 via seismic vessel *R/V Marcus G. Langseth* under a 6-km long streamer and a source array of 36 air guns with a total volume of 6600-cubic-inch, coined as MGL 0905-10 and MGL0905-27 (Figure 1). The data were acquired as part of multi-scale, cross disciplinary, on- and off-shore experiments, known as the Taiwan Integrated Geodynamics Research (TAIGER) project, with a general objective of tectonic quantification study of the Taiwan Island. Both seismic lines had opposite acquisition survey trends: MGL 0905-10 commenced from the wedge slope to the continental slope

(NE to SW trend), and inversely, MGL 0905-27 started from the continental slope to the wedge slope (SW to NE direction). A total of 468-hydrophones were spaced in every 12.5 m and common-depth point (CDP) spacing was 6.25 m. The shot interval was fixed at 50 m with a maximum of 60-fold coverage. The distance from the air gun to the nearest receiver was 164 m, with a time sampling of 2 ms and a time length of 15 s. Shot numbers started from 1211 to 5000 for MGL 0905-10, whereas in MGL0905-27, the shot number ranged from 1017 to 5916. Both streamers and sources were towed at 9-m and 8-m depths, respectively, with an average speed of 4.5–5.0 knots. Both reflection seismic data have been employed partially in shorter length by previous works on crustal-scale imaging in the Eurasian continental margin, slope of submarine Taiwan wedge, and abyssal plain of the SCS (Lester et al. 2012); crustal features of northeastern SCS (Yeh et al. 2012); crustal velocity crustal off SW Taiwan (Deng et al. 2012); crustal accretion study in the Manila trench accretionary wedge (Lester et al. 2013); imaging of hyper-extended rifted margin in northeastern SCS (McIntosh et al. 2013); crustal structure of rifted continental margin in southwestern offshore Taiwan (McIntosh et al. 2014); study on tectonic and sedimentary development in the northern margin of SCS (Liao et al. 2016); and study of deep-sea submarine erosion off southern Taiwan (Das et al. 2021). Out of these studies, only the first two references explicitly discussed the general processing workflow, especially, the de-multiple efforts to attenuate long-offset multiples in deep seismic reflection profiling.

The data were converted from SEG-D to SEG-Y and resampled to 4 ms sample interval. Trace editing was applied, followed by geometry application, sorted into CDP gathers, preliminary band-pass filter (2–4–60–80 Hz), and an amplitude correction for spherical divergence. Filter related to acquisition noises were applied to eliminate swell noises and noise bursts. A total number of nine receivers and three shots were missing from the raw data for both seismic lines. This missing information was interpolated to fill in the near-offset gap as a prerequisite step prior to the de-multiple procedures (Verschuur 2013). Brute-stack sections were derived by applying a constant water velocity (~ 1500 m/s) as normal move-out (NMO) velocity correction. The bin size is set to 6.25 m, which results in a maximum fold of approximately 59 traces. Direct waves were muted, followed by deghosting and predictive deconvolution. Twelve pairs of specific prediction length and operator length were determined from the autocorrelation of 15 traces to remove source wavelet and attenuate reverberations under various water depths (Table 1). WEMA and SRME, through multiple modeling and adaptive subtraction, were applied to attenuate the water bottoms, surface-related multiples, and near offset multiples. A radon filter was applied to eliminate multiples energy, primarily at far offset, based

Table 1. Compilation of prediction lag and operator length used for deconvolution. Number inside the bracket refers to the associated seismic line: (10) is MGL 0905-10 and (27) is MGL 0905-27.

Shot number	Bathymetry	Source wavelet removal		Reverberation removal		Approximate water depth two-way times (ms)
		Predicted lag (ms)	Operator length (ms)	Predicted lag (ms)	Operator length (ms)	
(10): 1211–2994	Lower slope	20	96	120	152	750–3700
(10): 2995–4882	Continental slope	20	100	68	148	3500–3800
(10): 4483–5000	Continental slope	20	172	100	252	3400–3500
(27): 1017–3338	Continental slope	20	180	116	152	3500–4600
(27): 3339–4360	Lower slope	20	176	124	156	3400–4500
(27): 4361–5916	Upper slope	20	68	120	224	800–3000

on velocity discrimination in the τ - p domain. To eliminate residual multiple energy, the F-K filter was applied through velocity discrimination in the F-K domain. The sequence of de-multiple methods was chosen based on trial and error, including the effectiveness of various de-multiple sequences under different water depths. A final time-variant frequency filter served to attenuate any artificial energy generated by the aforementioned de-multiple methods. Velocity analysis and its refinement analysis were performed after each de-multiple procedure to update the velocity field iteratively on every 500th CDP gather. For each velocity analysis, multi velocity function stack, semblances, and gathers were displayed interactively, allowing the determination of stacking velocity. Percentage stacks and NMO-corrected gathers were generated to double-check the velocity picking validity. This step was applied repetitively during each of the de-multiple stage. Post-stack Kirchhoff depth migration based on constrained Dix inversion (Koren and Ravve 2006) is deemed to produce the final stacking gather. The full re-processing workflow is depicted in Figure 2.

Effectivity of de-multiple methods

Predictive deconvolution

Predictive deconvolution utilizes the Wiener–Levinson algorithm to collapse source wavelets, sharpen seismic events, and extend the frequency bandwidth. Yilmaz (2008) defines the algorithm as to design an inverse filter from some number of autocorrelations that will remove the predictable event on seismic trace, including bubble noises and multiples. In practice, predictive deconvolution has been used to attenuate intra-bed and seafloor multiples (Berndt and Moore 1999, Yilmaz 2008, Lester and McIntosh 2012). Before the application, deconvolution operator length and prediction lag from an autocorrelation time gate are parameters that should be properly designated for optimum results. The autocorrelation time gate corresponds to the window over which autocorrelations of the traces are calculated. The deconvolution operator length is the time span over which the autocorrelation of the input seismic trace approximately equals the wavelet's autocorrelation. By analyzing the autocorrelation function, both short- and

long-period reverberations can be determined. Choosing the appropriate operator length and prediction lag are a matter of trial-and-error testing. Too-short operator lengths leave some residual energy in the auto-correlograms corresponding to the source wavelet and reverberations, whereas too-long operator lengths do not provide further improvement on the deconvolution output. Prediction lag controls the resolution of the deconvolution output. Shorter prediction lags cause more compression of the source wavelet, hence, increasing the bandwidth of the output with the collateral boost of the low- and high-frequency noise amplitudes. As the prediction lag increases, the whitening effectivity of deconvolution of the spectrum is reduced and the output auto-correlograms include more noises in non-zero lags. Selection of the second zero crossing point of auto-correlogram of the input seismogram is the general convention used in both seismic datasets with spectral whitening of the noise level kept at about 0.1 percent. In this study, predictive deconvolution was applied under shot gathers prior to velocity analysis. This would calculate the shot-consistent inverse filters from each source.

Since both seismic datasets span over complex tectonic settings, choosing a proper operator length and prediction lag require careful examination. Based on the bathymetry distribution, each seismic line was divided into several areas. Each area possesses a specific operator length and prediction lag for spiking the seismic wavelet, reverberations removal, and preliminary water-bottom multiple elimination (Table 1). Except for the first two objectives, multiple models for the latter are predicted by convolutional models through the information on water depth from a seismic trace header. Design windows were kept around 1–3 s. Time-variant band-pass filtering is applied afterward to reduce much of the residual reverberation energy. In general, deconvolution is successful at reducing the short period multiples related to the ghost and bubble effect, without introducing any artifacts and improving the spatial resolution in both seismic lines (Figure 3). Owing to the distortion of seismic signals propagating through long distances in large water depths, primary seafloor multiple is partially attenuated in stack gather (Figures 4 and 5) for both seismic lines. In the wedge slope of MGL0905-10, deconvolution is capable of reducing the

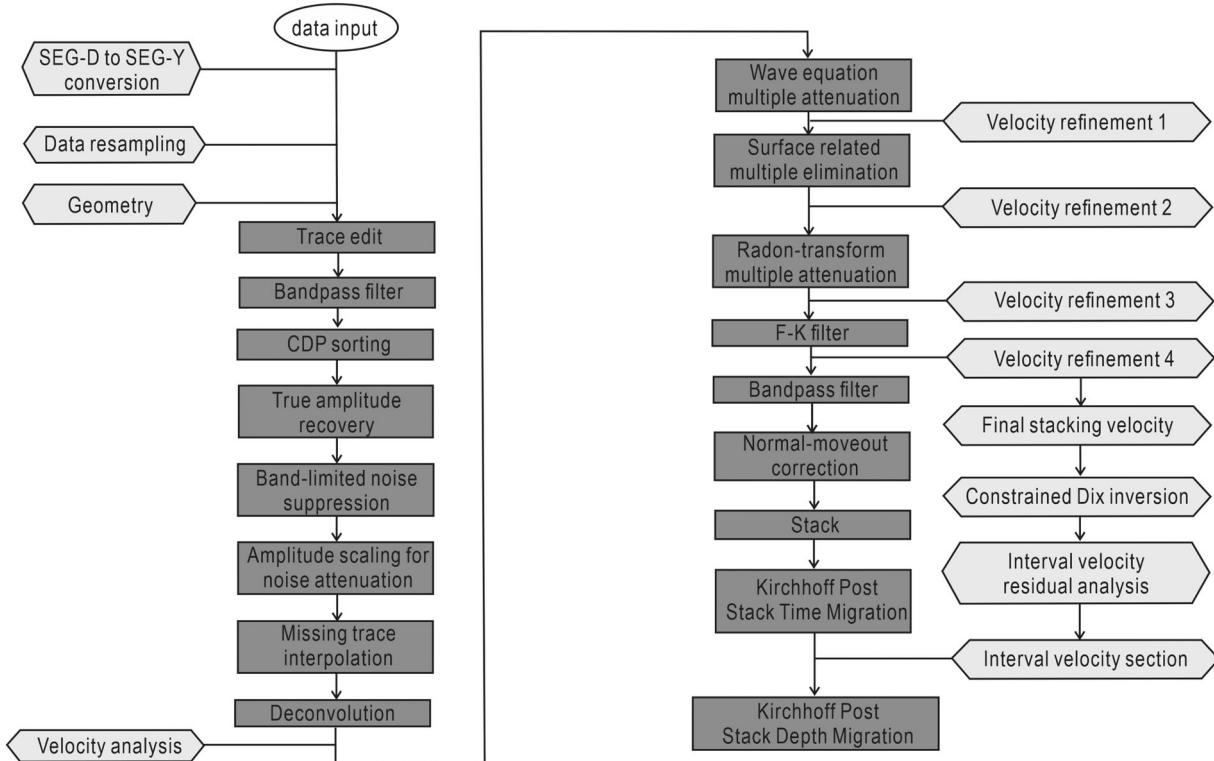


Figure 2. Schematic diagram of seismic re-processing for multi-channel seismic lines MGL 0905-10 and MGL 0905-27.

energy of sea-bottom and peg-leg multiples, significantly. Since the periodicity of multiples varies with the increasing offset due to normal move-out of the reflection hyperbolas, predictive deconvolution is efficient on short period multiples with a period less than 250 ms. By using the water depth-dependent prediction lag values, period variations of the multiples can be mitigated. However, predictive deconvolution could not remove the overall reverberations energy in the shallower upper wedge slope of MGL0905-27.

2D wave-equation multiple attenuation (WEMA)

WEMA performs multiple modeling and adaptive subtraction in the shot domain (Wiggins, 1988). Multiples are modeled by a downward continuation of the receivers to the multiple generating water bottom and an upward continuation of the receiver field by the same amount. This is followed by adaptive subtraction and receiver continuation back to the original receiver depths (Figure 6). The method makes no assumption about the character and complexity of the water bottom as long as its depth is known, giving simple water bottom multiples along with all the receiver side peg-leg multiples that are modeled properly. The most critical objectives in WEMA are to determine the form and amplitudes of the multiples accurately (Lu, Ursin, and Lutro 1999). In CDP gathers, seafloor multiple from previous de-multiple attempts is further attenuated after WEMA in lines MGL 0905-10 (Figure 4) and MGL 0905-27 (Figure 5). In general, WEMA is effective in

partially attenuating the sea-bottom multiples energy at all bathymetry and tectonic environments. The subtraction of predicted multiple takes place at the water bottom itself by taking into account the reflectivity effect (Wiggins, 1988). Short period multiples cannot be eliminated by WEMA, but their amplitudes are reduced.

2D surface-related multiple elimination (SRME)

According to Verschuur, Berkhouwt, and Wapenaar (1992), surface-related multiples can be kinematically predicted by the 2D surface integration of convolution of the pre-stack seismic traces at possible surface multiple reflection locations. By the use of Kirchhoff summations, the correct combination of an event to construct multiples is obtained automatically. Since it is independent of the velocity field and seafloor depth information, the Taylor expansion term is calculated as a convolution of input data with itself or a lower-order Taylor term (Lester and McIntosh 2012). When convolved with itself, the input seismic data predicts the first order Taylor term, which contains multiples only. The predicted multiple models can then be adaptively subtracted for original short gathers to remove records with free multiples. Since the iterative implementation of SRME in predicting the multiple models require extensive and heavy computation, this study only utilizes the first-order multiple prediction. Figures 4 and 5 show the influence of SRME after the previous de-multiple efforts in both seismic lines. Limited to only the first-order multiple prediction, SRME shows the least

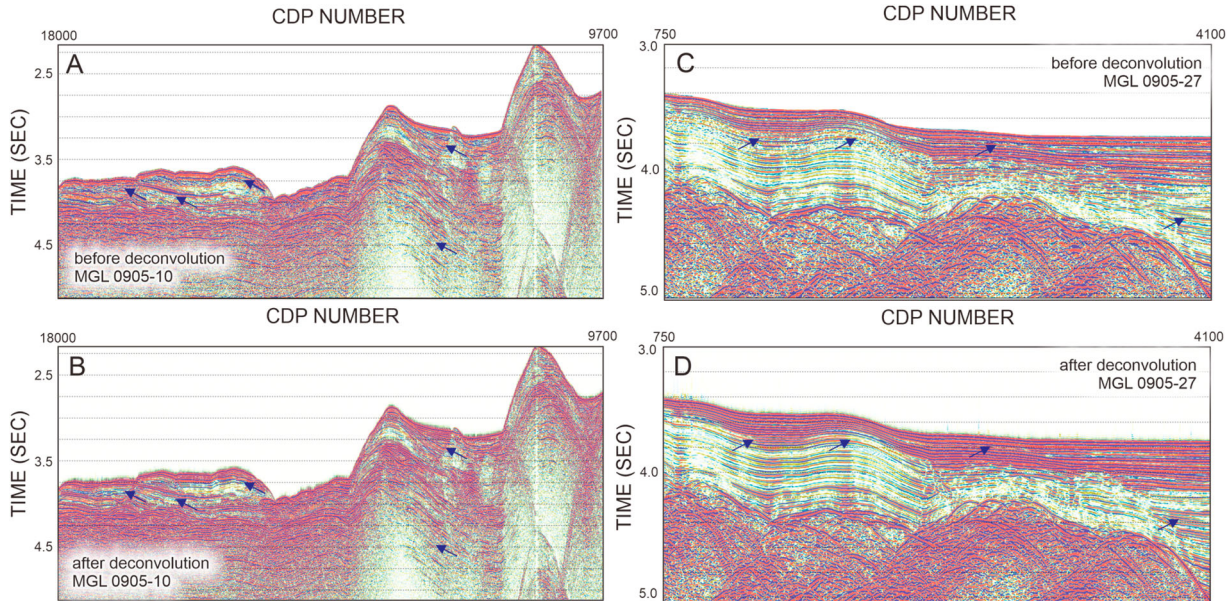


Figure 3. Comparing the influence of deconvolution in offset gathers between before (A, C) and after (B, D) the application. (A) and (B) depict comparison in MGL 0905-10, while B and D highlight discrepancy in MGL 0905-27. Notable improvement is shown by the dark blue arrows.

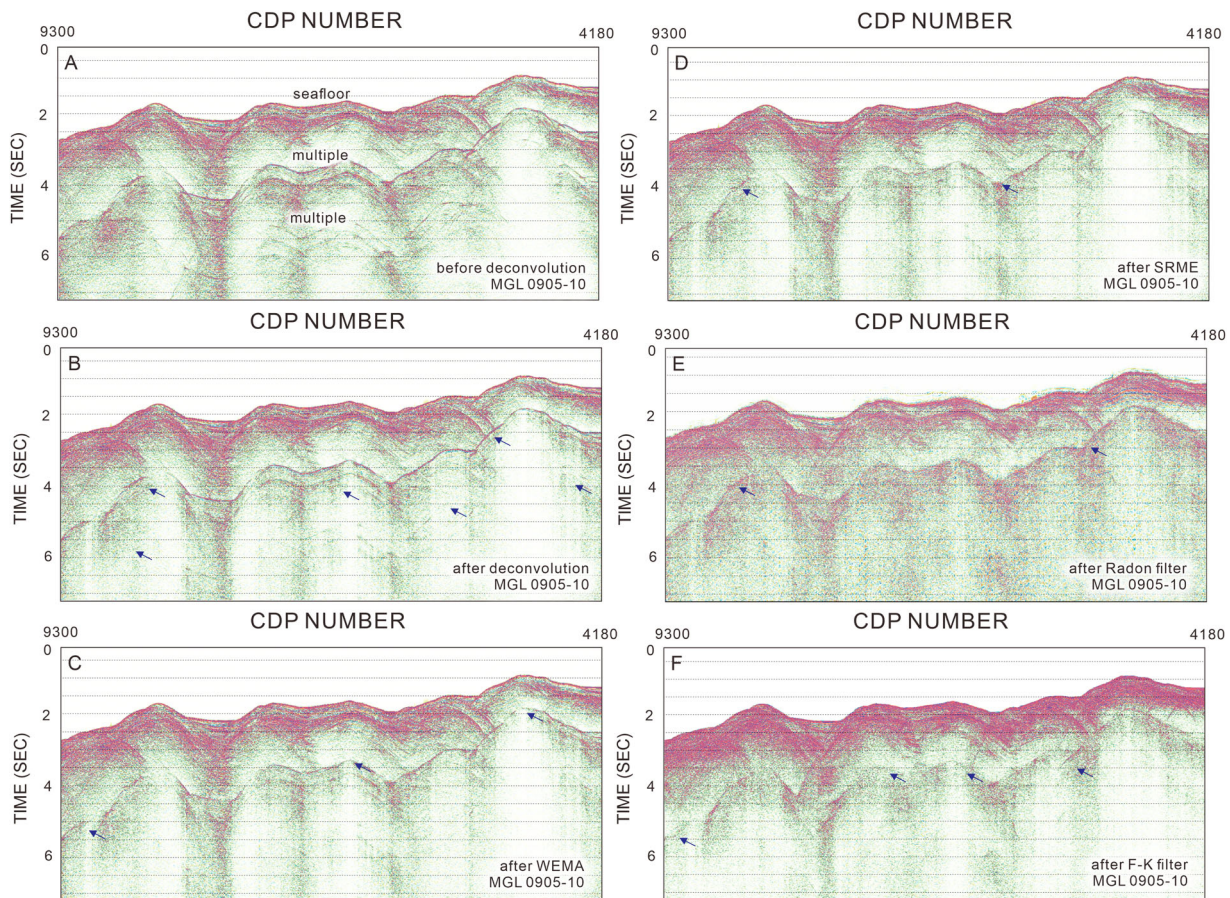


Figure 4. Comparability example of sequential de-multiple approaches in offset gather of the wedge slope area of MGL 0905-10: (A) pre deconvolution, (B) post deconvolution, (C) post WEMA, (D) post SRME, (E) post Radon filter, and (F) post F-K filter. Noteworthy improvements of each de-multiple technique are shown in dark blue arrows.

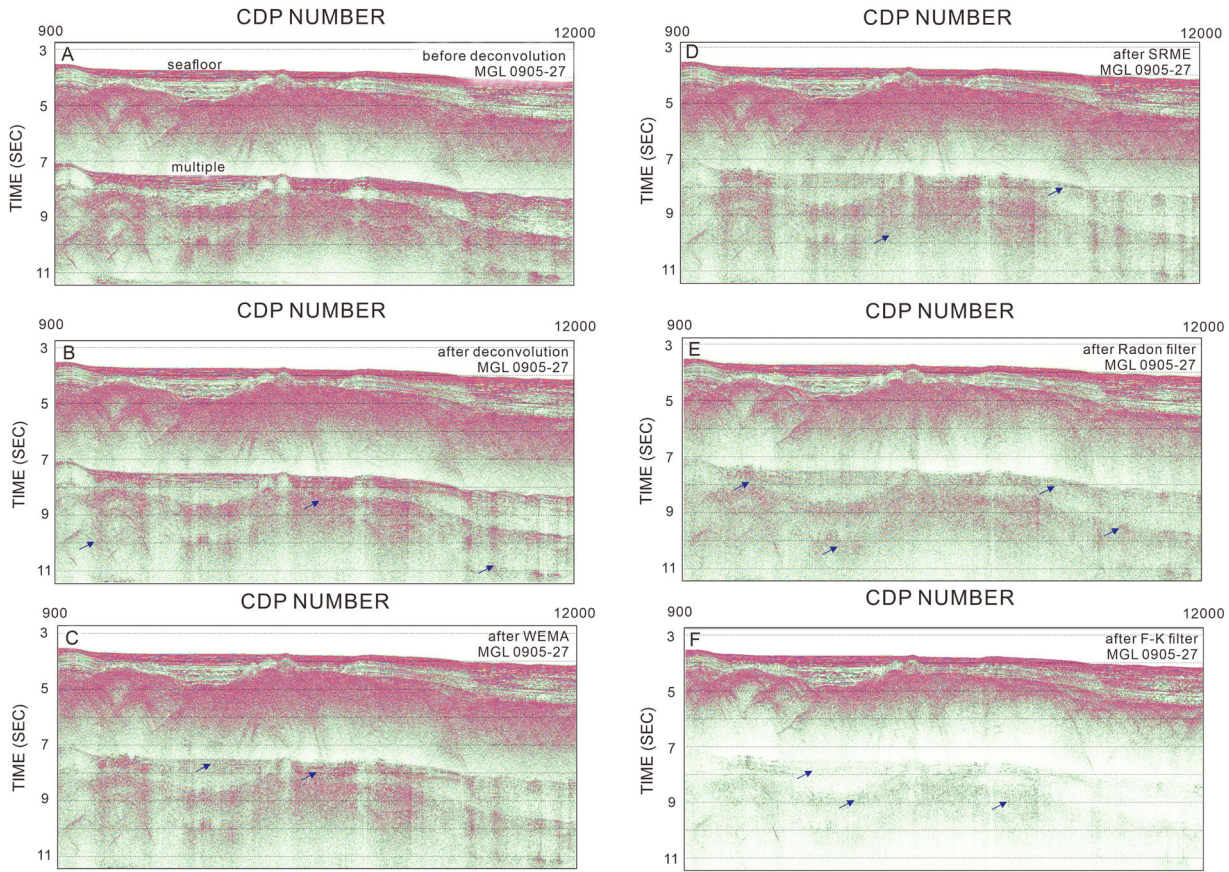


Figure 5. Comparison of sequential de-multiple efforts in offset gather of the continental slope area of MGL 0905-27: (A) before deconvolution, (B) after deconvolution, (C) after WEMA, (D) after SRME, (E) after Radon filter, and (F) after F-K filter. Blue arrows highlight the significant improvement of each de-multiple method.

impact of all the de-multiple efforts by weakening the interval multiple energy with minimal effect.

Radon filter

A radon filter incorporates parabolic Radon transform to attenuate multiple energy. The method performs a parabolic Radon transform on input gathers that have been corrected for a normal move-out. After the normal move-out correction with a proper root-mean square (RMS) velocity derived from primaries, the primary reflection events are expected to be flattened and the multiple reflection events may have residual move-outs. The primary and multiples events can be seen in the τ - p domain, where τ and p are coefficients defining the intercept time and the curvature of parabolic curves of NMO-corrected events in the input ensembles, respectively. It first performs a least-squares forward transform. The forward transform followed by an inverse transform without any filter in between yields a least-squares approximation to the input ensembles. A parabolic curvature of 1000 was set for a minimum P-wave velocity of 1450 m/s and maximum offset of 4000, giving a ray parameter of 800 with an increment of 2. Depending on the bathymetry, several inversion schemes have been developed for the least-squares forward transform, where each bathymetry possesses a

dedicated τ - p filter range. Assuming both the parameters in the model space and the noises in the data space have Gaussian distributions leads to a linear least-squares inversion scheme, denoted as Toeplitz inversion (Hampson 1986; Zhou and Greenhalgh 1994). After the forward transform, it zeros a user-specified zone of multiple energy in the τ - p domain, performs an inverse transform on the remaining primary energy back to the x - t domain, and replaces the original data with the remaining primary energy. Figures 4 and 5 infer the Radon filter process and its associated influence on multiple energy after the previous de-multiple trials for both seismic lines. Long period multiples are suppressed through the Radon filter in the continental and lower wedge slopes and improve the signal-to-noise ratio (S/N) at a greater depth. However, strong multiple energy in the upper wedge of MGL0905-10 is capable of surviving the effect of the Radon filter due to an imperfect inverse transform. This can be mitigated by having an expensive processing time, but hinders the practicality of the method.

F-K filter

The F-K filter defines a two-dimensional Fourier transform over time and space, where F is the frequency (Fourier transform over time) and K refers to the

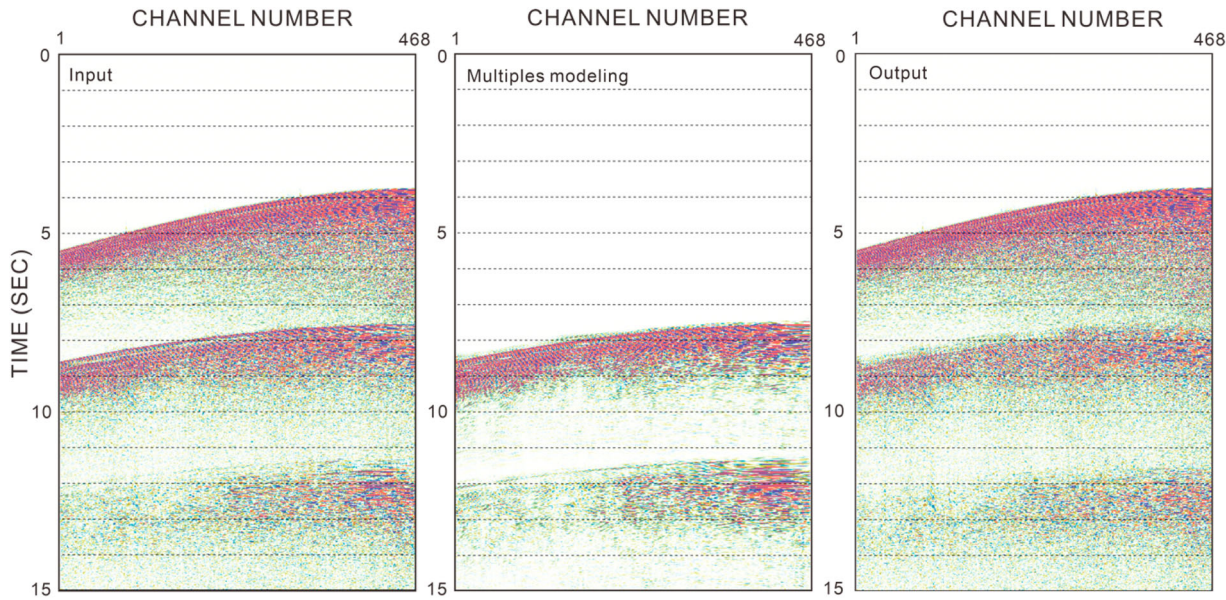


Figure 6. Example of multiple modeling via WEMA. The prediction is modeled by a downward continuation of the receivers to the multiple generating water bottom and an upward continuation of the receiver field by the same amount. This is followed by adaptive subtraction and receiver continuation back to the original receiver depths.

wavenumber (Fourier transform over space). Ryu (1982) described the first usage of the F-K filter for multiple removals by having NMO-corrected CDP gathers with a velocity function of the primary, such that the under-corrected multiples were mapped onto the positive wave numbers. Multiples were suppressed by muting the data for the positive wave numbers and inverse transforming the remaining perennial energy back to the x - t domain. Figures 4 and 5 show the effectiveness of the F-K filter on both seismic lines, where near-offset multiples and remaining multiple energy are further attenuated via the F-K filter. The filter is efficient to suppress the first and second order multiples at shallow water depth, but fails to attenuate higher order multiples due to the inadequate offset to separate primaries and multiples. Figures 7 and 8 highlight the improvement in velocity refinement after each step of de-multiple.

Limitation of de-multiple methods on stack gathers

The de-multiple methods do not come without limitation. The efficiency and success of each approach strongly depend on the criteria used to attenuate the multiples via the characteristic features of the multiples. While a number of various de-multiple methods must be tested to cope with different multiple targets, each de-multiple method is limited to certain boundary conditions. For example, multiple suppression based on periodicity and predictability requires specific assumptions to satisfy. Predictive deconvolution assumes a laterally invariant medium (Yilmaz 2008), which did not satisfy the tectonic environment of the study area (Figure 1). Long period multiples could not

be eliminated through deconvolution due to the primaries distortion when applying excessively long operator length (Yilmaz 2008). WEMA and SRME run on the assumption that shot and receiver geometry is a regular 2D line with equal shot and receiver interval. A shot location should exist at each receiver location, since every receiver location is also used as a source location (Verschuur, Berkhouw, and Wapenaar 1992). In a marine seismic survey, cable feathering and cross-line complexities are inevitable; therefore, the assumption could break down and reduce the accuracy of the seafloor and peg-leg multiples models. Coupled with the effects of spatial aliasing, error in water bottom reflectivity, and the lack of near traces, this could further perturb the predictability. Moreover, in SRME, interpolated missing shots and receivers for a complex subsurface may perturb multiple modeling (Verschuur, Berkhouw, and Wapenaar 1992). In this study, interpolated data from a total number of 12 missing receivers and shots in both seismic lines may influence the accuracy of multiple model predictability. On top of that, Wang (2004) described only the prediction of higher-order multiples will improve for a higher-order iteration, hence better multiple predictions. However, this study only utilized the first order iteration; consequently, underestimated multiple models could be expected.

On the other hand, multiple removal techniques by move-out discrimination are built upon two main assumptions: (1) multiples and primaries can be separated by parabolic move-out in the CDP-offset domain and (2) multiples and primaries can be mapped into different areas in the Radon and F-K domains. The first assumption works best for stratification with a minimal dip. However, this assumption is contravened since the Taiwan accretionary wedge was built upon crustal

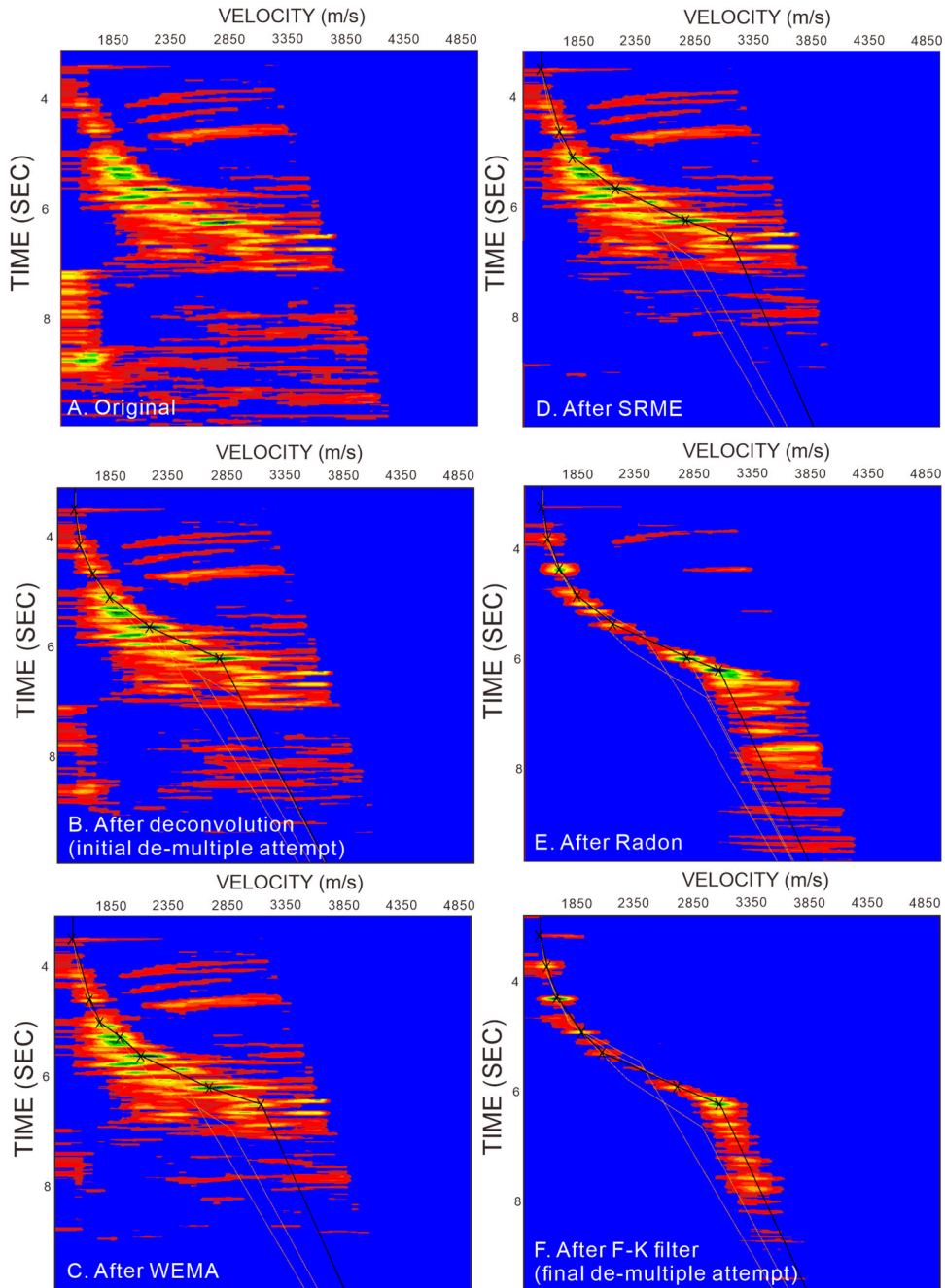


Figure 7. Comparison of velocity analysis before de-multiple (A) and after each de-multiple effort (B–F) in CDP 29751 of MGL 0905-10. Semblances of seismic noises are attenuated leaving primary semblances in a more discernible velocity gradient pattern.

shortening and thrust-related folds (Suppe 1984; Teng 1990), hence strong horizontal and vertical velocity contrasts over large structural complexities. Furthermore, reflection events in mildly dipping seafloor coupled with lateral geological variations, as in the continental slope, could exhibit non-hyperbolic behaviour (Verschuur 2013). Ray paths bounce at scattering points could generate multiples with a non-zero offset apex position (Hargreaves et al. 2003). In such a case, multiple suppression through move-out filtering would not suffice. Post the move-out correction, if the apex of multiples occurs at a non-zero offset, residual multiple energy will persist into the final stack. Due to similar move-out, the F-K filter may remove amplitudes

of primaries in near-offset traces. Furthermore, due to the geological nature of the wedge, the geometry of tilted strata is subject to tilted transverse isotropy (TTI). Kostecki (2011) suggested the direction of the isotropic plane inclined at a certain angle to hold a direct influence on elastic wave velocity. Without estimating the anisotropy parameters, TTI promotes overestimated velocity semblances, hence the impending error of multiple prediction models and move-out. Moreover, critical distortions caused by the TTI layers in isotropic seismic imaging are well documented in the literatures (Isaac and Lawton 1999; Vestrum, Lawton, and Schmid 1999). The influence of tilt promotes estimation ambiguity for velocity analysis and model

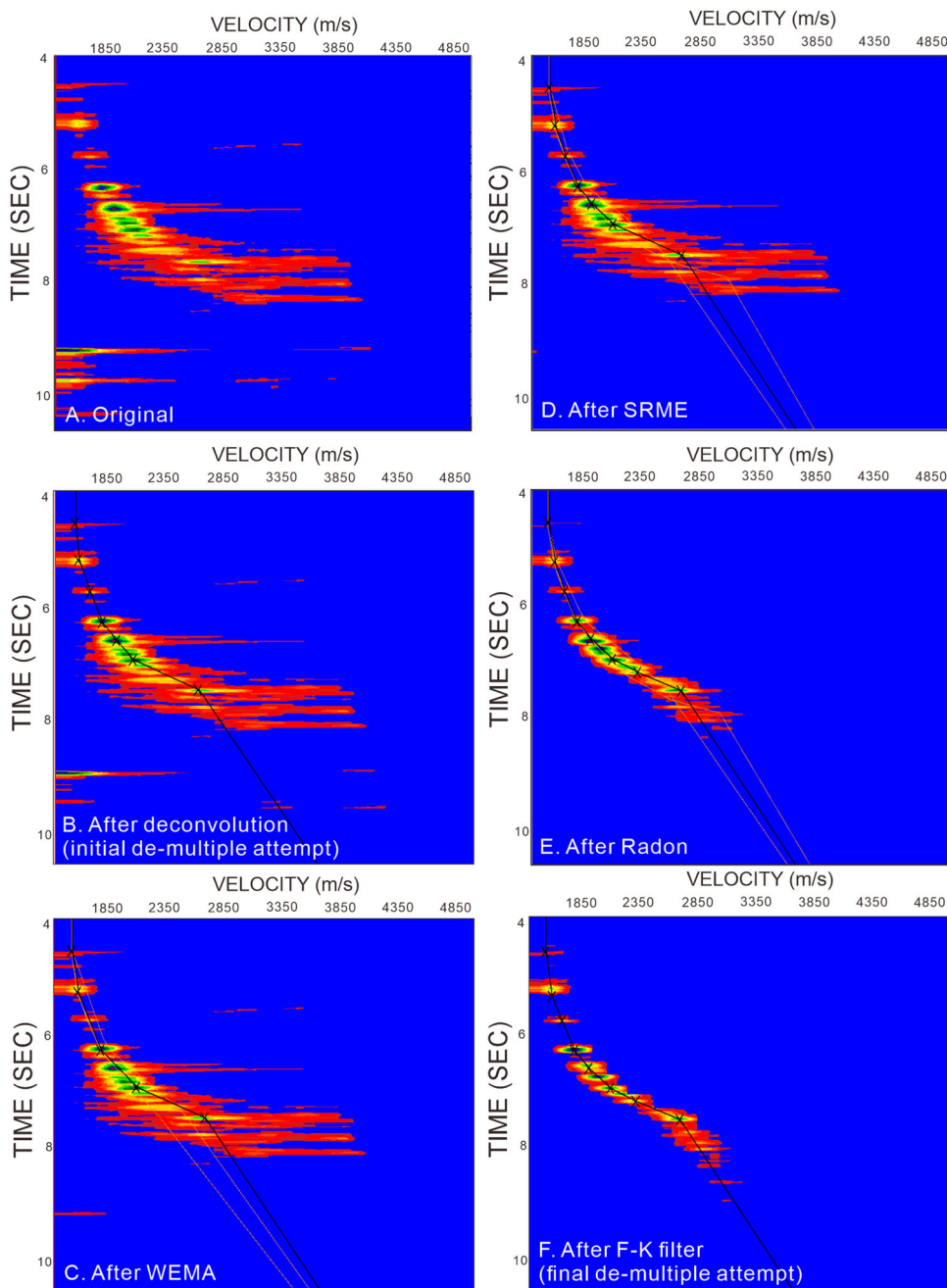


Figure 8. Velocity spectral improvement before de-multiple (A) and after each de-multiple effort (B–F) in CDP 16751 of MGL 0905-27. Semblances of seismic primaries become more discernible due to the weakened energy of seismic noises.

building in TTI media, such as in fold-and-thrust belts, including the Taiwan submarine accretionary wedge. The second assumption relies on the lower move-out velocity of multiples than the primaries at the same arrival times. This premise is valid if the subsurface velocity is monotonically increasing. However, if propagating velocities of the subsurface are changed such that a high velocity layer overlies lower velocity layers, multiples may present below the lower velocity layers and align with the primaries (Verschuur 2013). In this scenario, such multiples could not be removed through move-out filtering. Furthermore, the discrimination of primaries and multiples becomes vague as their events overlap each other. The presence of BSRs in the wedge

slope off southwestern Taiwan is characterized by its sudden drop in velocity (Lin et al. 2009b; Dirgantara et al. 2020a), promoting the abovementioned challenge of multiple removals at a shallower depth. CDP stacking exploits the final residual move-out differences between primaries and multiples after NMO correction, to suppress multiples. Depending on the number of traces involved, stacking may suppress a significant amount of coherent and incoherent noises and improve the S/N ratio up to 20 dB (Sheriff and Geldart 1995). Since small changes in NMO velocity may produce a significant amount of residual move-out differences at far offset, residual velocity analysis after each de-multiple application helps to improve the effective removal of

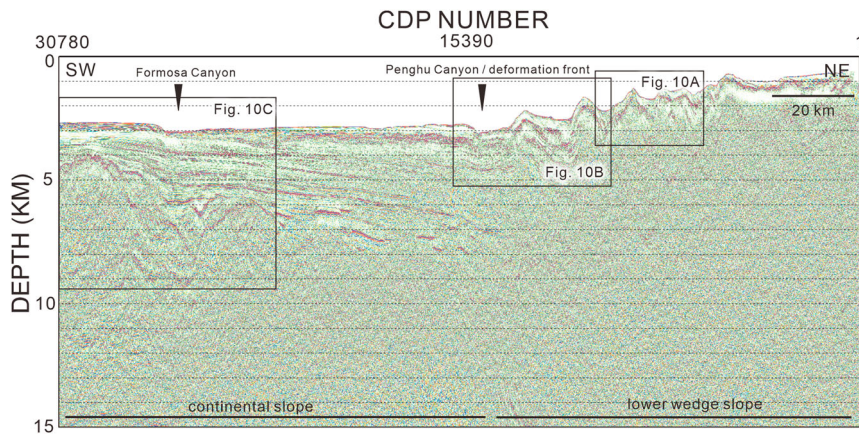


Figure 9. AGC-applied post-stack depth migration of MGL 0905-10 highlights the subsurface image under equalized amplitudes. Visual details are highlighted by the black squares, representing areas from the accretionary wedge slope and the continental slope.

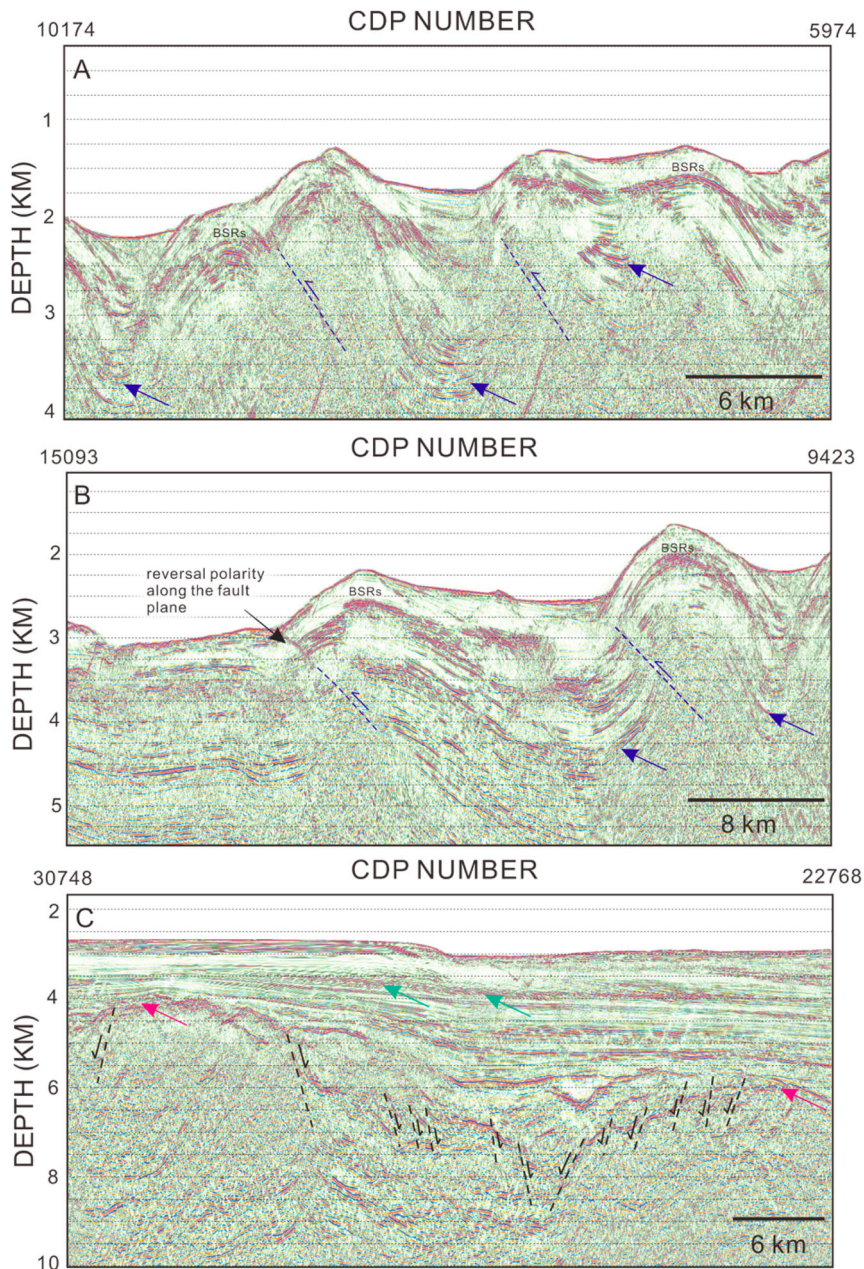


Figure 10. Close view results of post-stack depth migration of MGL 0905-10 as shown in (A, B) wedge slope area and (C) continental slope area from Figure 9. Interpretable reflection continuity in the syncline structure is shown by dark blue arrows. Thrust-and-fold belts are marked by repetitive in-sequence thrusts (blue dashed lines), often accompanied by a distinct reversal polarity along the plane. BSRs are present, inferring active gas hydrate systems of the area. Distinct boundaries of the basement are shown by red arrows. Progradational reflections are shown by green arrows. The graben system is shown by black dashed-lines.

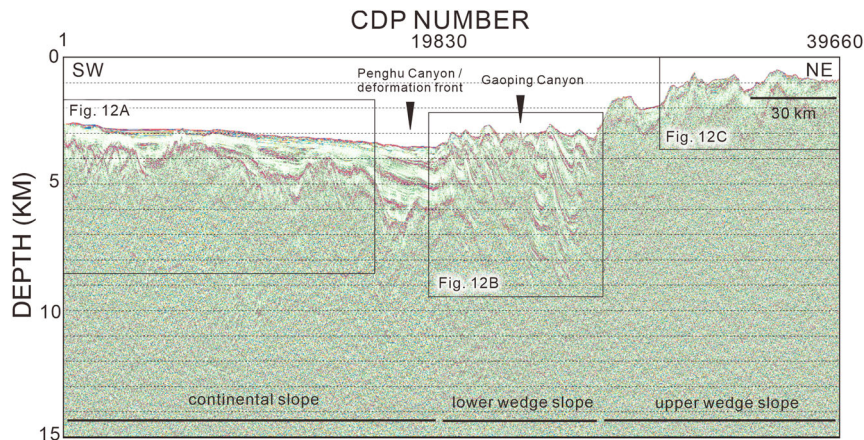


Figure 11. Post-stack depth migration of MGL 0905-27 under AGC displays the subsurface imaging under scaled amplitudes. The black squares highlight visual details in the areas of the continental slope and the accretionary wedge slopes.

multiples through stacking. De-multiple influences on velocity analysis exhibit a significant improvement as the degree of filter increases (Figures 7 and 8). Post stack depth migration introduces artifacts in the deeper structure which resemble typical results of migrating random noise. Residual multiples are vividly present in depth sections (Figures 9 and 11), notably in the wedge slope area. Das et al. (2021) postulated prominent submarine erosion developing in the upper slope domain (Figures 1 and 12) had exposed bedrock from paleoburial depth around 2–4 km. The proposed hypothesis is capable of promoting large reflection coefficient contrast between sea column and denuded bedrock, hence strong reverberation energy in the wedge slope area of MGL 0905-27.

Subsurface expression

The depth migrated sections span down to 15 km. Under equalized amplitudes, deeper reflection is highlighted in both depth-migrated sections. Extensive development of submarine thrust belts is well-imaged, inferred from the continuous reflections of repetitive eastward thrust-and-fold sequences in the wedge slope domain (Figures 10 and 12). Morphologically, the continental slope has an average water depth between 2500 and 3700 m, where its eastern boundary marks the deformation front. Intermediate bathymetry is visible for the lower wedge slope under a water depth between 2400 and 3000 m. A sudden bathymetry jump suggests the presence of an out-of-sequence thrust (Reed et al. 1992) or a termed splay fault in Lin et al. (2008), which separates the lower wedge slope from the upper wedge slope, exclusively in MGL0905-27 (Figure 11). This phenomenon is absent in MGL0905-10 as the seismic line does not cross the splay fault (Figures 1 and 9). The upper wedge slope extends around a water depth of 500–1500 m, with hints of distinct mud diapir intrusions (Figure 12). BSRs are present in the wedge slope domain, hinted by strong reversed polarity

cutting seismic reflections. Dip angles of thrust faults gradually decrease from the lower wedge slope toward the deformation front, suggesting multi stages of the in-sequence thrusts. Lateral accretion below the Formosa canyon hints at a possible canyon migration in the past (Figure 9). Mass transport deposits (MTDs) are identified by chaotic seismic and/or deformed reflectors. Hemipelagic or turbiditic sediments are interpreted from continuous parallel-subparallel reflections around 500 m to 1 km underneath the seafloor. Albeit scarce, intruded mud diapir through the seafloor in the lower wedge slope domain is hinted from the sea bottom-piercing morphology above chaotic reflection, suggesting the possibility of a thrust-related diapir (Figure 12). Deposited near the seafloor, sediment waves are distinguishable from layered, continuous to discontinuous, convex upward, and subparallel wavy reflectors. These sediments span over 2 km wavelength and a height of 40 m. Syn-rift graben structures are visible, possibly related to rifting events in the distal margin of north-eastern SCS during the Paleogene (Liao et al. 2016; Larsen et al. 2018) (Figure 9). In the continental slope domain, the distribution of basements is highlighted by a distinct impedance contrast that underlies the onlapping and down-lapping syn-rift parallel-subparallel reflections around 2–4 km below the seafloor. A series of buried seamounts and volcanic sills lie near the Penghu Canyon and the Manila Trench. The eastward dipping basement highlights the on-going convergence of the eastward moving Eurasian plate underneath the Taiwan accretionary wedge.

Conclusions

A cascade of de-multiple efforts on two MCS data highlights the challenges of multiple energy suppression on submarine crustal scale imaging in southwestern offshore Taiwan. Predictive deconvolution improves seismic resolution and suppresses sea-bottom reverberation energy in the rifted continental margin and the

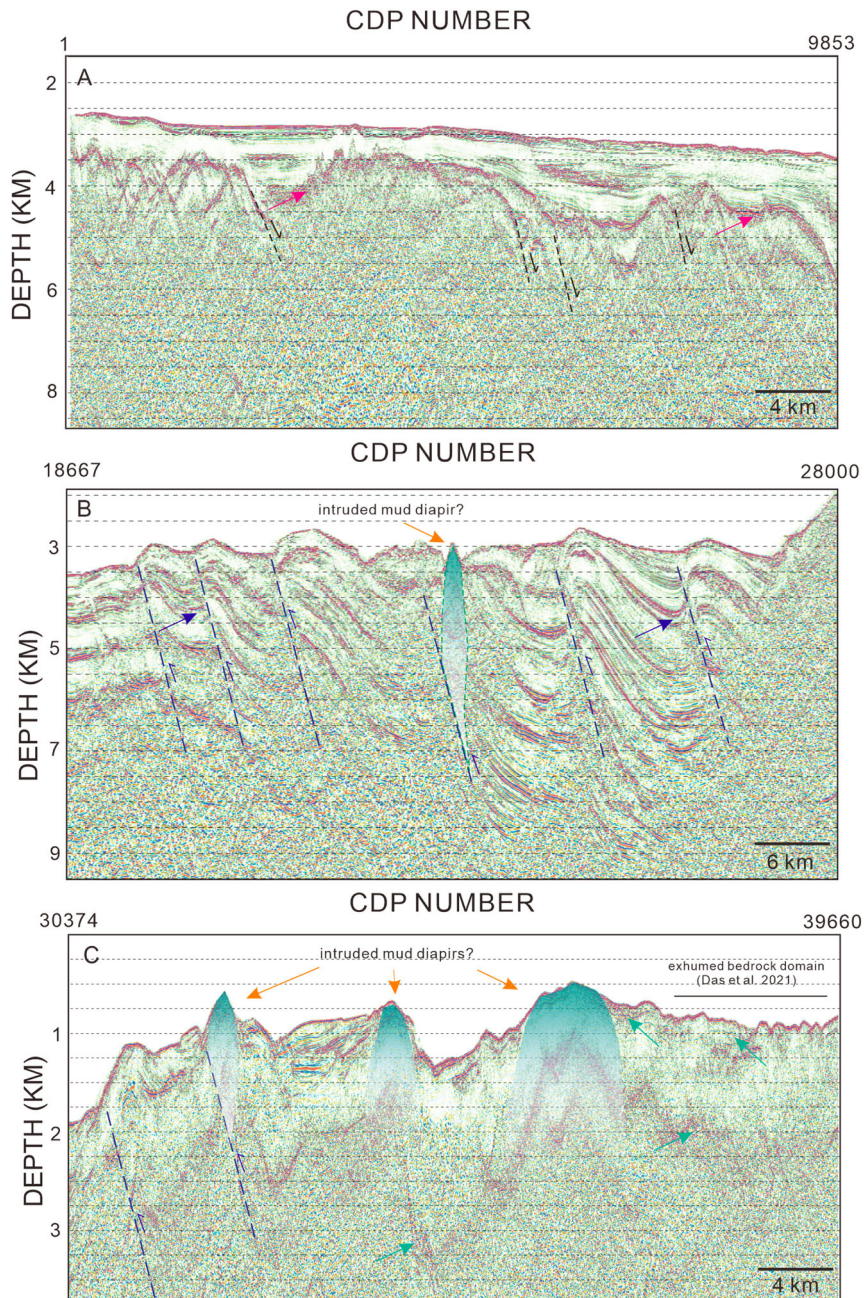


Figure 12. Zoom-in results of post-stack depth migration of MGL 0905-27 from Figure 11 as shown in the (A) continental slope area and (B, C) wedge slope area. Distinct basement reflection is shown by red arrows. In-sequence thrusts (dark blue dashed-lines) within the thrust-and-fold belts domain highlight the distinct displacement of reflection (dark blue arrows). Strong reflection of the top basement is shown by red arrows, whereas residual multiples energy is present (green arrows) in the upper slope. Intruded mud diapirs are shown by orange arrows. The graben system is shown by black dashed-lines.

lower accretionary wedge, but not in the upper wedge slope. WEMA, Radon filter, and F-K filter reduce the multiples energy both at the continental and wedge slopes, whereas SRME made minimal impact on both areas. Residual multiple energy infers the major influence of tectonic environment in coupling multiple energy. The overall re-processing strategy reveals a depth image of the complex subsurface structures off southwestern Taiwan. The graben system underlying episodic depositions of MTDs, hemipelagites/turbidites, and cut-and-fills features dominate the continental slope domain. Conversely, the compressional wedge

slope domain reveals extensive eastward dipping fold-and-thrust belts with dispersive BSRs and mud diapir distribution. While each de-multiple method comes with its own advantages and disadvantages, there is no single method capable of attenuating multiple energy under various tectonic settings and bathymetry.

Acknowledgements

The authors thank two anonymous reviewers for their fruitful and constructive feedback that has improved the quality of the manuscript.



Disclosure statement

No potential conflict of interest was reported by the author(s).

Funding

This work was supported by the Ministry of Science and Technology, Taiwan [grant number MOST109-2611-M-008-001].

References

- Berndt, C., and G.F. Moore. 1999. Dependence of Multiple-attenuation techniques on the geologic setting: A case study from offshore Taiwan. *Leading Edge* 18: 74–80.
- Boston, B., G.F. Moore, M.J. Jurado, and H. Sone. 2016. Deformation of the nankai trough inner accretionary prism: The role of inherited structures. *Geochemistry, Geophysics, Geosystems* 17: 485–500.
- Das, P., A.T. Lin, M.P. Chen, E. Miramontes, C.S. Liu, N.W. Huang, J. Kung, S.K. Hsu, R.K. Pillutla, and K. Nayak. 2021. Deep-sea submarine erosion by the kuroshio current in the Manila accretionary prism, offshore southern Taiwan. *Tectonophysics* 807: 228813.
- Deng, J.M., T.K. Wang, B.J. Yang, C.S. Lee, C.S. Liu, and S.C. Chen. 2012. Crustal velocity structure off SW Taiwan in the northernmost South China Sea image from TAIGER OBS and MCS data. *Marine Geophysical Research* 33, no. 4: 327–349.
- Deng, H., P. Yan, H. Liu, and L. Wenzao. 2006. Seismic data processing and the characterization of a gas hydrate bearing zone offshore of southwestern Taiwan. *Terrestrial, Atmospheric and Oceanic Sciences* 17 no. 4: 781–797.
- Dirgantara, F., H.T. Chiang, A.T. Lin, C.S. Liu, and S.C. Chen. 2020b. Depositional influence of submarine channel migration on thermal properties of the Lower Fangliao Basin, offshore southwestern Taiwan. *Marine Geophysical Research* 41, no. 1: 1–23.
- Dirgantara, F., A.T. Lin, C.S. Liu, C.C. Lin, and S.C. Chen. 2020a. Gas-hydrate systems and gas volumetric assessment in the Lower Fangliao Basin, Taiwan accretionary wedge. *Journal of Petroleum Geology* 43, no. 1: 27–48.
- Gong, C.L., Y.M. Wang, S. Xu, K.T. Pickering, X.C. Peng, W.G. Li, and Q. Yan. 2015. The northeastern South China Sea margin created by the combined action of down-slope and along-slope processes: Processes, products and implications for exploration and paleoceanography. *Marine and Petroleum Geology* 64: 233–249.
- Hall, R. 2002. Cenozoic geological and plate tectonic evolution of SE Asia and the SW pacific: computer-based reconstructions, model and animations. *Journal of Asian Earth Sciences* 20, no. 4: 353–431.
- Hampson, D. 1986. Inverse velocity stacking for multiple elimination. *Canadian Journal of Exploration Geophysicists* 22: 44–55.
- Hargreaves, N., B. VerWest, R. Wombell, and D. Trad. 2003. Multiple attenuation using an apex-shifted Radon transform. In *73rd Annual International Meeting SEG Expanded Abstracts*, 1929–1932.
- Hsu, H.H., C.S. Liu, H.S. Yu, J.H. Chang, and S.C. Chen. 2013. Sediment dispersal and accumulation in tectonic accommodation across the Gaoping Slope, offshore SW Taiwan. *Journal of Asian Earth Sciences* 69: 26–38.
- Isaac, J.H., and D.C. Lawton. 1999. Image mispositioning due to dipping TI media: A physical modeling study. *Geophysics* 64, no. 4: 1230–1238.
- Koren, Z., and I. Ravve. 2006. Constrained Dix inversion. *Geophysics* 71, no. 6: R113–R130.
- Kostecki, A. 2011. Tilted transverse isotropy. *Nafta-Gaz* 11: 769–776.
- Larsen, H.C., G. Mohn, L. Zhong, et al. 2018. Rapid transition from continental breakup to igneous oceanic crust in the South China Sea. *Nature Geoscience* 11: 782–789.
- Lee, Y.H., C.C. Chen, T.K. Liu, H.C. Ho, H.Y. Lu, and W. Lo. 2006. Mountain building mechanisms in the Southern Central Range of the Taiwan Orogenic Belt: From accretionary wedge deformation to arc-continent collision. *Earth and Planetary Science Letters* 252, no. 3–4: 413–422.
- Lester, R., and K.D. McIntosh. 2012. Multiple attenuation in crustal-scale imaging: examples from the TAIGER marine reflection dataset. *Marine Geophysical Research* 33, no. 4: 289–305.
- Lester, R., K. McIntosh, H.J.A. van Avendonk, L. Lavier, C.S. Liu, and T.K. Wang. 2013. Crustal accretion in the Manila trench accretionary wedge at the transition from subduction to mountain-building in Taiwan. *Earth and Planetary Science Letters* 375: 430–440.
- Liao, W.Z., A.T. Lin, C.S. Liu, J.N. Oung, and Y. Wang. 2014. Heat flow in the rifted continental margin of the South China Sea near Taiwan and its tectonic implications. *Journal of Asian Earth Sciences* 92: 233–244.
- Liao, W.Z., A.T. Lin, C.S. Liu, J.N. Oung, and Y. Wang. 2016. A study on tectonic and sedimentary development in the rifted northern continental margin of the South China Sea near Taiwan. *Interpretation* 4, no. 3: 47–65.
- Lin, C.C., A.T. Lin, C.S. Liu, G.Y. Chen, W.Z. Liao, and P. Schnurle. 2009b. Geological controls on BSR occurrences in the incipient arc-continent collision zone offshore southwest Taiwan. *Marine and Petroleum Geology* 26, no. 7: 1118–1131.
- Lin, A.T., C.S. Liu, C.C. Lin, P. Schnurle, G.Y. Chen, W.Z. Liao, L.S. Teng, H.R. Chuang, and M.S. Wu. 2008. Tectonic features associated with the overriding of an accretionary wedge on top of a rifted continental. *Marine Geology* 255, no. 3–4: 186–203.
- Lin, A.T., A.B. Watts, and S.P. Hesselbo. 2003. Cenozoic stratigraphy and subsidence history of the South China Sea margin in the Taiwan region. *Basin Research* 15, no. 4: 453–478.
- Lin, A.T., B. Yao, S.K. Hsu, C.S. Liu, and C.Y. Huang. 2009a. Tectonic features of the incipient arc-continent collision zone of Taiwan: Implications for seismicity. *Tectonophysics* 479, no. 1–2: 28–42.
- Liu, C.S., I.L. Huang, and L.S. Teng. 1997. Structural features off southwestern Taiwan. *Marine Geology* 137, no. 3–4: 305–319.
- Liu, C.S., P. Schnurle, Y. Wang, S.H. Chung, S.C. Chen, and T.H. Hsiuan. 2006. Distribution and characters of gas hydrate offshore of southwestern Taiwan. *Terrestrial, Atmospheric and Oceanic Sciences* 17, no. 4: 615–644.
- Lu, G., B. Ursin, and J. Lutro. 1999. Model-based removal of water layer multiple reflections. *Geophysics* 64, no. 6: 1816–1827.
- Ludmann, T., H.K. Wong, and P.X. Wang. 2001. Plio-Quaternary sedimentation processes and neotectonics of the northern continental margin of the South China Sea. *Marine Geology* 172, no. 3–4: 331–358.
- Lundberg, N., D.L. Reed, C.S. Liu, and J. Lieske, Jr. 1992. Structural controls on orogenic sedimentation, submarine Taiwan collision. *Acta Geologica. Taiwanica* 30: 131–140.
- McIntosh, K., L. Lavier, H. van Avendonk, R. Lester, D. Eakin, and C.S. Liu. 2014. Crustal structure and inferred rifting processes in the northeast South China Sea. *Marine and Petroleum Geology* 58: 612–626.
- McIntosh, K., H. van Avendonk, L. Lavier, R. Lester, D. Eakin, F. Wu, C.S. Liu, and C.S. Lee. 2013. Inversion of

- a hyper-extended rifted margin in the southern Central Range of Taiwan. *Geology* 41 no. 8: 871–874.
- Reed, D.L., N. Lundberg, C.S. Liu, and B.Y. Kuo. 1992. Structural relations along the margin of the offshore Taiwan accretionary wedge: implications for accretion and crustal kinematics. *Acta Geologica Taiwanica* 30: 105–122.
- Ryu, J.V. 1982. Decomposition (DECOM) approach applied to wave field analysis with seismic reflection records. *Geophysics* 47: 869.
- Seno, T., S. Stein, and A.E. Gripp. 1993. A model for the motion of the Philippine Sea plate consistent with NUVEL-1 and geological data. *Journal of Geophysical Research* 98, no. B10: 17941–17948.
- Sheriff, R.E., and L.P. Geldart. 1995. *Exploration seismology*. Cambridge: Cambridge University Press.
- Shipley, T.H., K.D. McIntosh, E.A. Silver, and P.L. Stoffa. 1992. Three-dimensional seismic imaging of the Costa Rica accretionary prism: structural diversity in a small volume of the lower slope. *Journal of Geophysical Research* 97: 7912–7926.
- Sun, S.C., and C.S. Liu. 1993. Mud diapir and submarine channel deposits in offshore Kaohsiung-Hengchun, southwest Taiwan. *Petroleum Geology of Taiwan* 28: 1–14.
- Suppe, J. 1981. Mechanics of mountain building and metamorphism in Taiwan. *Memoir of the Geological Society of China* 4: 67–89.
- Suppe, J. 1984. Kinematics of arc-continent collision, flipping of subduction, and back-arc spreading near Taiwan. *Memoir of the Geological Society of China* 6: 21–33.
- Teng, L.S. 1990. Geotectonic evolution of late Cenozoic arc continent collision in Taiwan. *Tectonophysics* 183, no. 1–4: 57–76.
- Verschuur, D.J. 2013. *Seismic multiple removal techniques: Past, present and future*. Netherlands: EAGE.
- Verschuur, D.J., and A.J. Berkhouwt. 2015. From removing to using multiples in closed-loop imaging. *Leading Edge* 34, no. 7: 744–759.
- Verschuur, D.J., A.J. Berkhouwt, and C.P.A. Wapenaar. 1992. Adaptive surface-related multiple elimination. *Geophysics* 57, no. 9: 1166–1177.
- Vestrup, R., D.C. Lawton, and R. Schmid. 1999. Imaging structures below dipping TTI media. *Geophysics* 64, no. 4: 1239–1246.
- Wang, Y. 2004. Multiple prediction through inversion: A fully data-driven concept for surface-related multiple attenuation. *Geophysics* 69, no. 2: 547–553.
- Wiggins, W. 1988. Attenuation of complex water-bottom multiples by wave-equation-based prediction and subtraction. *Geophysics* 53, no. 12: 1527–1539.
- Yeh, Y.C., S.K. Hsu, W.B. Doo, J.C. Sibuet, C.S. Liu, and C.S. Lee. 2012. Crustal features of the northeastern South China Sea: Insights from seismic and magnetic interpretations. *Marine Geophysical Research* 33, no. 4: 307–326.
- Yilmaz, O. 2008. *Seismic data analysis*. Tulsa: Society of Exploration Geophysics.
- Yu, S.B., H.Y. Chen, and L.C. Kuo. 1999. Velocity field of GPS stations in the Taiwan area. *Tectonophysics* 274, no. 1–3: 41–59.
- Yu, H.S., and Z.Y. Huang. 2006. Intraslope basin, seismic facies and sedimentary processes in the Kaoping slope, offshore SW Taiwan. *Terrestrial, Atmospheric and Oceanic Sciences* 17, no. 4: 659–677.
- Zhou, B., and S.A. Greenhalgh. 1994. Linear and parabolic τ -p transforms revised. *Geophysics* 59, no. 7: 1133–1149.